Atomic and electronic structure of the $Fe_3O_4(111)/MgO(111)$ model polar oxide interface

V. K. Lazarov,[1,*] M. Weinert,[1] S. A. Chambers,[2] and M. Gajdardziska-Josifovska[1,†]
[1]*Department of Physics and Laboratory for Surface Studies, University of Wisconsin-Milwaukee, P.O. Box 413, Milwaukee, Wisconsin 53201, USA*
[2]*Fundamental Science Division, Pacific Northwest National Laboratory, P. O. Box 999, MS K8-93, Richland, Washington 99352, USA*
(Received 13 May 2005; revised manuscript received 29 August 2005; published 1 November 2005)

High-resolution transmission electron microscopy (HRTEM) and density functional calculations are used to study the effect of interface polarity on the atomic and electronic structure of the prototype $Fe_3O_4(111)/MgO(111)$ polar oxide interface. We show that atomically abrupt interfaces exist between the MgO(111) substrate and magnetite (111) film in regions separated by Fe nanocrystals, and propose a solution for this oxide-oxide interface structure. Comparisons of experimental HRTEM images with calculated through-focus and through-thickness images for model interface structures suggest metal-oxygen-metal (i.e., Mg—O—Fe) interface bonding with octahedral (B) coordination of the first Fe monolayer, rather than the combination of tetrahedral-octahedral-tetrahedral (ABA) stacking also found in Fe_3O_4. First-principles calculations for all the different models find metal-induced gap states in the interface oxygen layer. Consistent with the HRTEM results, the MgO—Fe_3O_4 interface stacking $\cdots$,4Mg/4O/**4Mg/4O/3Fe$_B$**/4O/$Fe_AFe_BFe_A$,$\cdots$, is calculated to be the energetically most favorable, and effectively screening the MgO(111) substrate surface polarity. The data and calculations exclude mixing of Mg and Fe across the interface, in contrast to the commonly invoked mechanism of cation mixing at compound semiconductor polar interfaces.

DOI: 10.1103/PhysRevB.72.195401 PACS number(s): 68.55.Jk, 68.47.Gh, 68.37.Lp, 81.15.Aa

I. INTRODUCTION

The question of the stability of polar interfaces is closely related to that of polar surfaces of ionic solids: the apparent presence of electric dipole moments in the unit cell perpendicular to the surface and/or interface naively leads to an electrostatic instability. The structure of polar oxide surfaces appears to be determined by the tendency to cancel, or at least minimize, the net electric dipole moment perpendicular to the surface (e.g., Ref. 1, and references therein). Studies of compound semiconductor interfaces based on electrostatic models[2,3] exclude the possibility of atomically abrupt polar semiconductor heterointerfaces, predicting a huge dipole moment and subsequent charge accumulations at such abrupt interfaces. The fact that ionicity is more pronounced in oxides than in compound semiconductors has led us to suggest that polarity would have a significant effect on the growth and structure of polar oxide films on polar oxide substrates.[4] Controlled growth of magnetite films has been the subject of intense studies inspired by its many technological applications, including spin valves and magnetic tunneling junctions (Ref. 5, and references therein). The very small lattice mismatch between Fe_3O_4 and MgO of 0.33% provides an almost perfect epitaxial match, making MgO a prime candidate for growth of magnetite based spintronic structures, but also for fundamental studies of oxide heterointerfaces.

In our first experimental study of a model polar oxide interface we found that the MgO(111) polar surface affects the epitaxial growth of a $Fe_3O_4(111)$ polar film by inducing phase separation within the magnetite (111) film and at the interface.[4] This type of phase separation was not observed when $Fe_3O_4(111)$ is grown on metallic Pt(111),[6] or when $Fe_3O_4(100)$ is grown on neutral oxide MgO(001) substrates.[7,8] The phase separation, with the creation of Fe (and FeO) nanoinclusions, was also found in molecular beam epitaxy (MBE) growth of magnetite (111) on alumina (0001) substrates.[9] Farrow *et al.*[9] also conducted systematic studies of iron oxides growth, structure, and magnetic properties using a range of Fe fluxes and oxygen partial pressures. They found a suppression of Fe nanocrystals in $Fe_3O_4(111)$ grown on the polar $Al_2O_3(0001)$ surface using much more oxidizing conditions than those needed for a single phase magnetite growth on MgO(001). The observed difference was ascribed to the use of different substrates, without discussion of the oxide substrate polarity. By comparing magnetite grown under the same oxygen plasma-assisted molecular beam epitaxy conditions on the polar and neutral surfaces of magnesia under the same substrate temperature and surface preparation conditions, Lazarov *et al.*[4] showed that the substrate polarity was a driving force for the phase separation.

In this paper, we explore atomic and electronic interface stabilization mechanisms for the model $Fe_3O_4(111)/MgO(111)$ polar oxide heterointerface in regions that are not covered with Fe nanocrystals, as indicated in Fig. 1. We combine high-resolution transmission electron microscopy (HRTEM) and density functional theory (DFT) calculations to explore the effect of polarity on the atomic and electronic structure, and to determine the interface structure via comparison with calculated HRTEM images.

II. METHODS

MgO single crystal substrates were oxygen plasma cleaned and annealed in an ultrahigh vacuum at 800 °C, resulting in an MgO(111)-(1×1)-OH terminated surface structure.[10] Fe_3O_4 films were grown by oxygen plasma-assisted molecular beam epitaxy, and characterized by x-ray photoelectron spectroscopy and transmission electron mi-

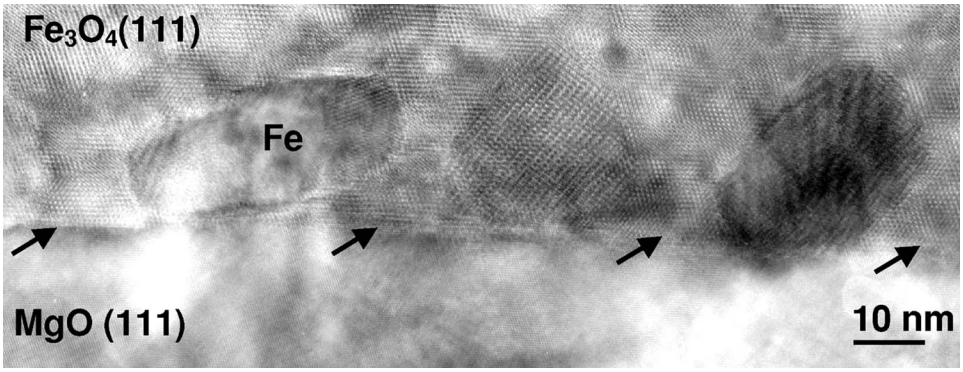

FIG. 1. Broader-view HRTEM image of the $Fe_3O_4(111)$/MgO(111) interface showing abrupt oxide-oxide interface regions (identified by the arrows) separated by regions with Fe(110) and $Fe_3O_4(001)$ nanocrystals in the magnetite film.

croscopy and diffraction.[4] A Hitachi H-9000 NAR microscope, with 1.8 Å point resolution at 300 keV, was used for HRTEM imaging of the cross sectional specimen of the $Fe_3O_4(111)/MgO(111)$ interface in the $[1\bar{1}0]$ and $[11\bar{2}]$ directions, two mutually perpendicular zone axis. The experimental parameters used for HRTEM imaging were 10 nm defocus step, 5–10 mrad beam convergence, 1.5 eV electron energy spread, 0.67 mm spherical aberration, and 1.4 mm chromatic aberration. Numerous defocus series of 15–20 HRTEM images were taken under such conditions, starting the series a few steps over-focus, then going through minimum contrast, Scherzer defocus and continuing up to three times of optimum (Scherzer) defocus. Images were recorded with a slow scan 1024×1024 pixel Gatan charge-coupled device camera, using Digital Micrograph acquisition software.

The HRTEM image calculations were done using the multislice method,[11] implemented in the Java version of the Electron Microscopy Software (EMS) package.[12] Supercells were constructed for four different model interface structures projected in two different zones. Magnetite has twice the repeat unit of MgO, requiring 4 and 12 atomic layers in the magnetite repeat unit along the $[1\bar{1}0]$ and $[11\bar{2}]$ directions, rather than 2 and 6 layers that are sufficient for MgO in these two directions. Thus, the number of the interface slices was defined by the number of magnetite repeat units, and the propagation distance between the slices was chosen to be equal to the bulk $(1\bar{1}0)$ and $(11\bar{2})$ distances of 1.470 and 0.856 Å, respectively.

The spin-polarized DFT calculations were done in slab geometry using the full-potential linearized augmented plane wave (FLAPW) method as implemented in *flair*.[13] The generalized gradient approximation (GGA) (Ref. 14) for exchange correlation was used for the interface supercells, giving a good match between the calculated (8.387 Å) and experimental (8.396 Å) Fe_3O_4 lattice constants, corresponding to (2×2) MgO(111) layers, i.e., 4 atoms per layer in the two-dimensional (2D) unit cell. Exploratory calculations used 6 layers of MgO as a substrate, while other calculations typically used between 9–15 layers of MgO. To model the surfaces in a repeated slab approach, both symmetric (MgO slabs with Fe—O layers on both sides, i.e., the same surface terminations) and asymmetric (different surface terminations) were used; to remove the effect of artificial interslab dipole interactions for the asymmetric slabs, symmetric supercells that included two oppositely oriented asymmetric slabs were also used. (With this setup, the calculated results become independent of the vacuum regions, in contrast to the case when asymmetric slabs are repeated. In addition, comparison of the calculated results for several of the more important interfaces using different computational cells, including different surface terminations, found consistent interface properties.) The Brillouin zone sampling was adjusted to maintain a constant density in reciprocal space, corresponding to ~3000–6000 k points/atom in the full Brillouin zone. (This density corresponds to ~100 k points in the irreducible zone for a one atom per unit cell cubic material.) In order to make meaningful comparisons among different models, the atomic positions were relaxed according to the calculated forces and total energies.

III. RESULTS AND DISCUSSIONS

A. Interface models

Both MgO and Fe_3O_4 are cubic systems: MgO has the rock salt structure with a lattice constant of 4.217 Å and two atoms per primitive unit cell; magnetite has the inverse spinel structure with a lattice constant of 8.396 Å and 14 atoms per primitive unit cell. Both magnetite and MgO have hexagonal symmetry along the common polar [111] direction. The MgO stacking along the [111] direction has alternating Mg and O planes stacked in the characteristic *abc* fcc stacking. Similarly, the magnetite stacking along the [111] direction is again a fcc stacking of a $(4O/3Fe_B/4O/Fe_AFe_BFe_A)$ unit, with two alternating types of Fe units—$3Fe_B$ and $Fe_AFe_BFe_A$—between the O planes, where Fe_A and Fe_B denote an Fe atom in the tetrahedral (A) and octahedral (B) positions, respectively.

Based on the two distinct Fe(111) planar units (three Fe atoms per unit) in the magnetite bulk structure, two models of the interface emerge immediately: (1) Interface B, is initiated with a monolayer of $3Fe_B$ (i.e., $4Mg/4O/3Fe_B/4O$); and (2) Interface ABA, is initiated with the three layer unit $Fe_AFe_BFe_A$ (i.e., $4Mg/4O/Fe_AFe_BFe_A/4O$). The two models are shown in Fig. 2 in a $[11\bar{2}]$ projection. Submodels can be created by introducing vacancies at the ABA interface; for example, interface BA, defined as $4O/Fe_BFe_A/4O$, and interface A, defined as $4O/Fe_A/4O$.

The electrostatic treatment of polar oxide surfaces and interfaces usually assigns bulk charges to the metal and oxy-

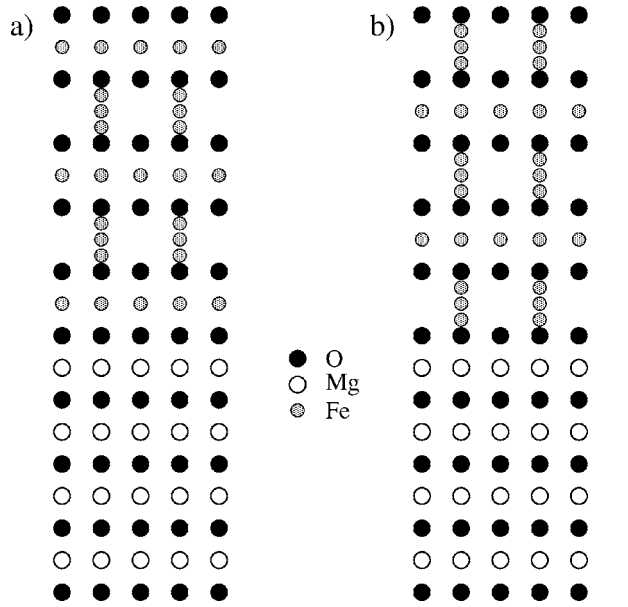

FIG. 2. Model interfaces for the $Fe_3O_4(111)/MgO(111)$ interface in the $[11\bar{2}]$ projection: (a) interface B initiated with a monolayer of Fe in the octahedral position ($3Fe_B$); (b) interface ABA, initiated with Fe in the tetrahedral position ($Fe_A/Fe_B/Fe_A$).

gen ions to calculate the electric dipole moments in the polar direction, and will depend on how the repeat unit cell is started. The values obtained by this approach are shown in Table I for MgO and for four possible magnetite (111) stacking repeat units. These results indicate that interface A should have the lowest dipole moment per magnetite repeat unit, and it is also the only model in which the film dipole moment is oppositely oriented to the substrate. Dipole moment minimization is often considered the main stabilization criterion in the simple electrostatic picture, suggesting that this polarity minimization might be able to offset the energy cost of creating interface vacancies in model A. However, first-principles studies of insulating polar oxide surfaces have found that the electronic degrees of freedom create the possibility for 2D surface metallization, electron transfer, and drastic polar oxide surface relaxations (e.g., review Ref. 1, and references therein). Therefore it is expected that the electrostatic predictions also might be misleading in the case of interfaces.

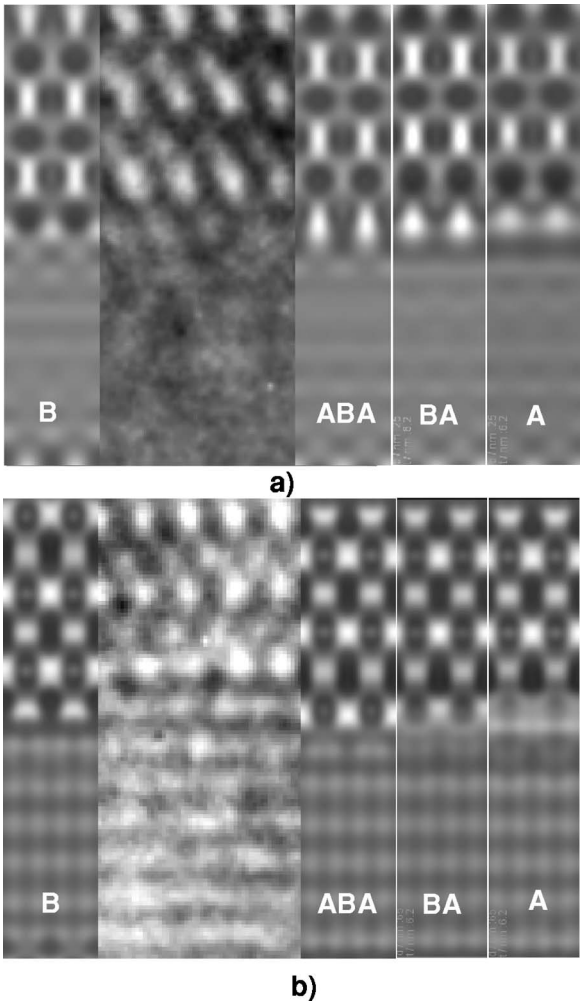

FIG. 3. Image comparison between experimental and calculated (for interface models B, ABA, BA, and A) HRTEM images in the $[11\bar{2}]$ zone at a constant thickness of ~6 nm, and two different defocus settings: (a) −25 nm and (b) −65 nm.

B. $Fe_3O_4(111)/MgO(111)$ atomic structure from HRTEM experiments and simulations

In Fig. 3, examples of experimental HRTEM images compared to calculated images in the $[11\bar{2}]$ zone for the interface B model (on left) and interfaces ABA, BA, and A (on right)

TABLE I. Electric dipole moments (in Debyes, $1D = 3.336 \times 10^{-30}$ C m) per unit area and volume using bulk interlayer spacings and ionic charges for various repeat units normal to the MgO(111), and $Fe_3O_4(111)$ bulk-terminated surfaces.

	μ (D)	μ (D/Å^2)	μ (D/Å^3)	Dipole orientation
Mg/O	11.72	1.52	0.62	↑
B: $3Fe_B/4O/Fe_AFe_BFe_A/O$	100.59	3.40	0.69	↑
ABA: $Fe_AFe_BFe_A/4O/3Fe_B/4O$	88.76	3.01	0.61	↑
BA: $Fe_BFe_A/4O/3Fe_B/4O/Fe_A$	29.58	1.00	0.20	↑
A: $Fe_A/O/3Fe_B/4O/Fe_BFe_A$	29.58	1.00	0.20	↓

TABLE II. Cross correlation coefficient (CCC) between experimental and calculated HRTEM images from models B, ABA, BA, and A, as shown in Fig 3.

	B	ABA	BA	A
Images, Fig. 3(a)	0.62	−0.32	−0.49	−0.25
Images, Fig. 3(b)	0.57	0.33	0.1	0.18

are shown. The experimental images zoom in on the same defect-free interface region from larger area HRTEM images that are first aligned using nonperiodic image features, such as Fe nanocrystals, lattice defects, and/or film surface edges. This alignment is needed to compensate for specimen drift during the acquisition of through-focal series of images. Based on MgO minimum contrast at defocus values of −25 and −65 nm, the specimen thickness at the particular regions is estimated to be 6 ± 1 nm. All model supercells start with an equal number of MgO layers, requiring that all simulated images be aligned at the MgO end. The calculated images have better resolution and contrast than the experimental ones, as the calculations do not include noise, image drift, residual astigmatism and beam tilt, or higher order aberrations. The calculations do not aim to simulate fully all details of the experimental image, but rather the goal is to compare the main image features that are sensitive to changes of the interface structure. At a defocus of −25 nm [Fig. 3(a)], Interface B is the best match, the other three models being noticeably misaligned with the experimental magnetite lattice fringes. At a defocus of −65 nm [Fig. 3(b)], all interface models are aligned but the contrast variations in interface B are again a better fit to the experimental image contrast than interface ABA-derived models. Through-focal image matching in the $[1\bar{1}0]$ zone (not shown here) also favors Interface B as a better match to the experimental HRTEM images.[15]

Visual comparison between the experimental and calculated images gives adequate conclusions when the difference between the calculated images are large, resulting in obvious lattice misalignments for the poor fit models in Fig. 3(a). To add some quantitative measure, cross correlation coefficients (CCC) were calculated between the experimental and calculated images of Figs. 3(a) and 3(b) with results given in Table II. CCC correlates pixel to pixel intensities between two images, giving +1 when the two images are identical in both periodicity and contrast (i.e., fully cross correlated), and −1 when there is no correlation between the images. Experimental HRTEM images of solved structures are known to have lower contrast than calculated images even when their periodicities present a perfect fit. This difference in intensity is called the "Stobbs factor," and it is under much current investigation and debate. Hence, we do not expect a CCC value close to +1 for the best fit model B in Table II, but rather a highest positive value compared to the competing models, as is clearly shown for both defocus values.

Next we address the uniqueness of the atomic structure of the interface. HRTEM images from interface regions that contain steps on the MgO(111) substrate are used to determine whether the initial stacking of magnetite is unique or not. Figures 4(a) and 4(b) show the magnetite growth on

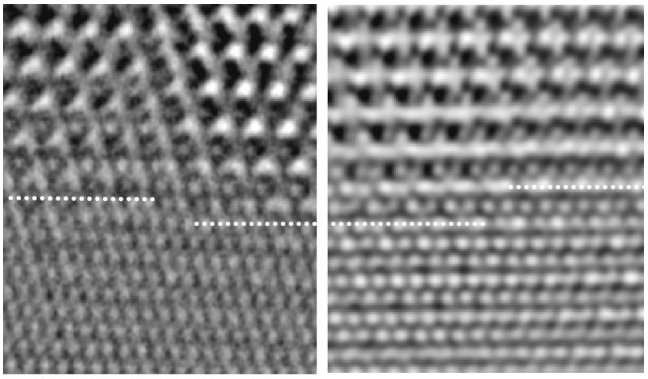

FIG. 4. HRTEM images of the interface for regions with steps on the MgO(111) surface: (a) For an odd number (one) of bilayers at the step, lattice misalignment is observed in Fe_3O_4 film, indicative of a grain boundary. (b) No grain boundaries are present when the step height consists of an even number (two) of Mg—O bilayers.

substrate terraces separated by a step height corresponding to an odd and even number of Mg—O bilayers, respectively. When magnetite grows on neighboring terraces separated by an odd number, a grain boundary appears in the film separating the grains that nucleate on these terraces. No grain boundary is created when the step has an even number of Mg—O bilayers. This evidence indicates that magnetite has the same (unique) stacking on the different terraces. Equivalent inverse domain grain boundaries were also observed when GaN grows on stepped SiC,[16] where the cause of their appearance, just as in the present case of $Fe_3O_4(111)$ grown on odd-stepped MgO(111), is that there is a preferred stacking at the interface, rather than a random one.

The hydrogen termination of the starting polar MgO surface[10] poses a third interesting question about the interface structure: Does H remain at the interface or not? Intensity profiles [Fig. 5(b)] from the HRTEM interface image [Fig. 5(a)] do not show interplanar distances across the interface that are substantially different than the expected MgO and $Fe_3O_4(111)$ spacings modeled by interface B [Fig. 5(c)]. Our calculations for an H monolayer at the interface predict an increase of the O—Fe interplanar distance from the bulk average value of 1.22 Å to 2.6 Å. Image simulations with H at the interface also find a poor fit with the experimental HRTEM images, as shown by the simulated intensity profile in Fig. 5(d). Thus, the experimental interface HRTEM images, together with the total energy calculations, justify the neglect of H in the presented interface models.

Our previous TEM experiments[4] and the HRTEM experimental images presented here rule out interface faceting and interface mixing as possible stabilization mechanisms, and indicate that the $Fe_3O_4(111)$ film has a preferred stacking, implying a unique interface structure. Based on comparisons of experimental and calculated images, interface B generates the best fit to the experimental data. Within the electrostatic model there is no obvious explanation why this interface should be more favorable than the other interfaces considered. We next present the results of the first-principles total

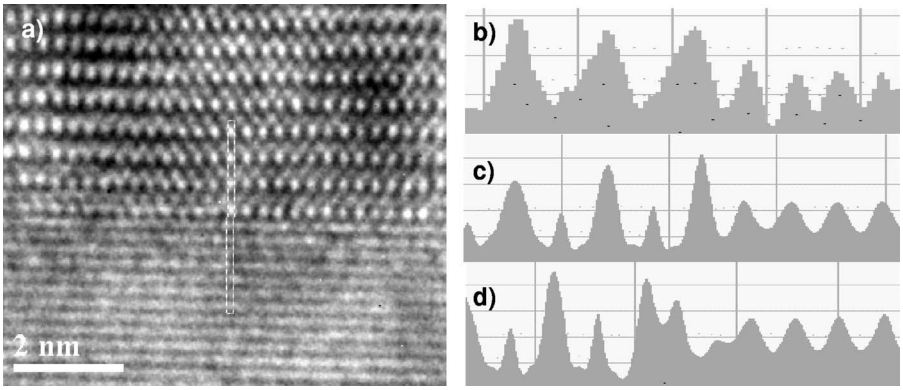

FIG. 5. (a) HRTEM image from the $Fe_3O_4(111)/MgO(111)$ interface in the $[11\bar{2}]$ zone. Intensity profiles along the [111] direction across the interface from: (b) the experimental image, (c) a simulated image of model B, and (d) a simulated image with one monolayer of H inserted between MgO and the Fe_3O_4 of the interface B model.

energy calculations performed for the four discussed interface models.

C. Total energy and electronic structure from DFT calculations

By using first-principles calculations we are able to probe the electronic and structural properties in ways that are not easily (if at all) accessible to experiment, including making comparisons to structures that might not exist experimentally. The two basic interface models, B and ABA, can be modeled by equal numbers of Mg, Fe, and O atoms using the following stackings: $(4Mg/4O)_N/3Fe_B/4O/Fe_AFe_BFe_A/4O/3Fe_B$ and $(4Mg/4O)_N//Fe_AFe_BFe_A/4O/3Fe_B/4O/Fe_AFe_BFe_A$, where N corresponds to the number of MgO bilayers in the substrate. Total energy calculations indicate that interface B has a lower energy than interface ABA by 4.1 eV per interface. This result is consistent with the HRTEM structure determination that favors interface B. The two types of suprecells have different Fe interface structures and different surface terminations for the Fe_3O_4 surface. The main energy difference between the two models is due to the different binding energies of the first Fe layer on MgO: If the three interface Fe_B atoms are moved from their octahedral positions to the $Fe_AFe_BFe_A$ (tetrahedral-octahedral-tetrahedral) positions, the energy cost is $\sim$1.0 eV per Fe atom, indicating that $\sim$3 eV of the energy difference between the B and ABA supercells is due to the initial magnetite growth; the additional energy difference is predominantly due to the different Fe_3O_4 surface terminations. A more direct measure of the initial preference for the B interface is given by calculations that considered the initial stages of the growth of the first layer (interface) of Fe, i.e., comparison of 1, 2, and 3 Fe atoms on a (2×2) O-terminated MgO; the $3Fe_B$ overlayer was favored by a 0.99 eV/Fe atom compared to an $Fe_AFe_BFe_A$ overlayer, consistent with the previous results. Although we have not calculated the growth of subsequent layers individually, the observed alternation between the B and ABA Fe layers is expected in order to maintain the preferred bulk coordination of the Fe_3O_4 structure. The models of the BA and A interfaces, generated by introducing appropriate vacancies in the ABA interface model, are less binding by $\sim$3.5 eV/Fe relative to the ABA interface and bulk Fe (one limit for the Fe chemical potential). The structural relaxations are similar to the ABA model and interface gap states are found in these models also. Although experimental conditions can change the chemical potentials significantly (on the order of a few eV) and affect the relative stability of different phases, for reasonable expected variations in the Fe chemical potential, interface B will still be preferred.

Total energy calculations also were performed to analyze the ability of Fe to displace the monolayer of H that initially terminates the unreconstructed MgO(111) substrate surface. We have considered two simple models. (1) A Fe monolayer bonded to the OH-terminated MgO; and (2) a H monolayer on top of a Fe monolayer bound to the O-terminated MgO. The second configuration is energetically more favorable by $\sim$1.5 eV per H atom. This calculation predicts that Fe can replace H at the interface because the Fe—O bond is stronger than the O—H one. This result rationalizes the absence of a distinct H monolayer in the HRTEM observations and simulations of the MgO/Fe_3O_4 interface. It remains to be determined if H is desorbed into the gas phase, migrates to interstitial lattice sites at the interface or in the bulk, or acts as a surfactant in the growth of the polar oxide film.

Interface mixing of Fe and Mg atoms was also considered by switching the positions of one interface Mg with one of the three interface Fe_B atoms. Although both cations maintain their octahedral coordination, this type of mixing is not energetically favorable, costing a $\sim$1.9 eV/Fe—Mg pair. Interchanging Fe and O interface atoms is even less favorable ($\sim$8–10 eV/Fe—O pair) because the strong Fe—O and Mg—O bonds are replaced by weaker metal-metal and O—O bonds. Although atomic mixing at polar semiconductor interfaces has been proposed based on semi-classical theories as a solution to the interface polarity problem, our calculations suggest that interface mixing in the $MgO—Fe_3O_4$ case does not promote the stability of the polar interface.

Figure 6 shows the average Coulomb potentials along the [111] polar direction for an O-terminated MgO surface, a monolayer of Fe_{3B} (the first Fe layer of Interface B) on MgO, and an Fe_3O_4 overlayer on MgO(111). As can be seen from the figure, the potential in the MgO reaches the bulklike values closer to the interface and/or surface for both the Fe_{3B} and Fe_3O_4 overlayers, compared to the O-terminated surface, in large part due to metallic Fe states induced at the interface. While there is a high density of surface states at the bottom of the gap for the O-terminated surface,[10] it is not simply the number of states in the gap, but rather their character that is

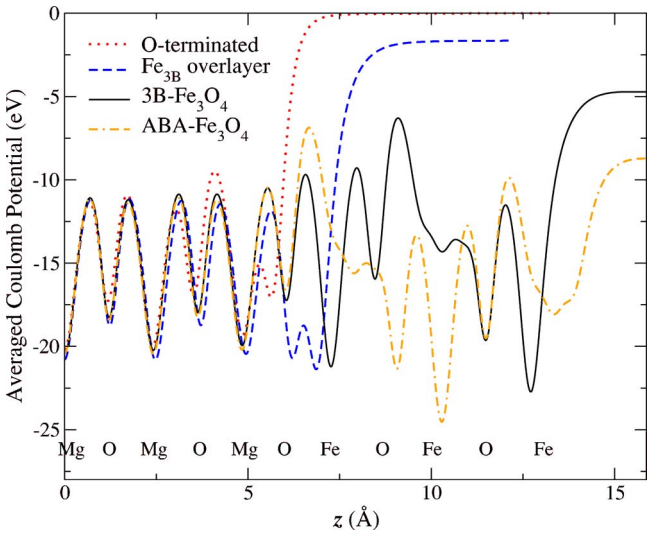

FIG. 6. (Color online) The planar-averaged Coulomb potentials along the [111] direction for an O-terminated MgO substrate (from a 41 layer MgO film); for an (11-layer) MgO substrate with a $3Fe_B$ overlayer (the initial Fe layer deposition), a $3Fe_B/4O/Fe_AFe_BFe_A/4O/3Fe_B$ overlayer (3B-Fe_3O_4), and a $Fe_AFe_BFe_A/4O/3Fe_B/4O/Fe_AFe_BFe_A$ overlayer (ABA-Fe_3O_4). All results were obtained using symmetric supercells and include structural relaxations. The curves were shifted to approximately align the bulk MgO potentials; the differences in the averaged potentials at large distances are a measure of the differences in the work functions for those surface terminations.

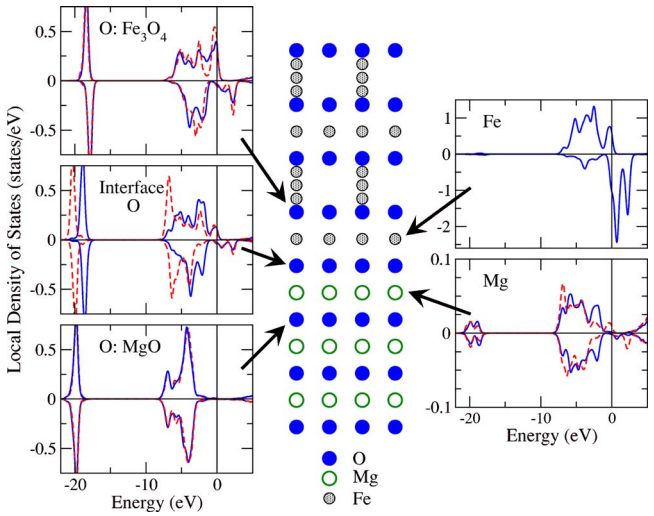

FIG. 7. (Color online) Local spin-resolved density of states for different atomic sites around the interface for the interface B model. Majority (minority) spin LDOS are plotted as positive (negative) values. Solid (dashed) lines denote sites with three (one) symmetry equivalent atoms per layer. Note the different vertical scales for the O, Fe, and Mg sites.

important: Small charge rearrangements and/or polarizations can be quite effective in screening,[17] and for this system the Fe electrons play an important role. Other interfaces, including single layers of Fe, Fe_{2B}, and Fe_{ABA} show similar behavior, i.e., the electronic degrees of freedom are very effective in screening the substrate-film polarity because of the metallic-like states at the interface.

What is perhaps most striking for the polar 3B-Fe_3O_4 overlayer is how well the MgO potential merges into the Fe_3O_4 one; without the labels of where the interface is, one might naively expect the interface to be at around the Fe_{ABA} layer. (The largest changes in the averaged potential are actually internal to the Fe_3O_4 layer, between the O and Fe_{ABA} layers, similar to the large changes seen for the ABA-Fe_3O_4 overlayer.) This matching of the average potentials across the interface is a result of electronic effects associated with the local atomic structure, which in turn cause structural relaxations at the surfaces; there are noticeable shifts in the atomic positions of the Mg, O, and Fe atoms nearest the interface among the three related cases. For interface B, the Mg—O bond lengths at the interface for the (one) threefold oxygen are reduced by (2.8%) 5% compared to the bulk MgO values, and there is a buckling of the oxygen of about 0.22 Å; the interface Fe_B—O bondlengths are expanded by 10% relative to bulk Fe_3O_4. (For interface ABA, the Mg—O bonds are even shorter, being between 7.1% and 7.7% shorter than in the bulk, the interface Fe_A—O bond is 6% larger than the bulk value, and the O layer buckling is slightly smaller, only ~0.07 Å.)

The calculated local density of states (LDOS) around the interface layers for interface B is shown in Fig. 7. Because of the symmetry of the interface, the four (O or Mg) atoms per layer separate into a group of three equivalent atoms (solid lines) and a single one (dashed line); the differences between these two sites is a measure of effect of the broken symmetry due to the interface on the electronic properties since in bulk MgO and Fe_3O_4 all the oxygen (and Mg) sites are equivalent. On the MgO side of the interface, the LDOS for the two inequivalent oxygens two layers from the interface (O:MgO) are essentially indistinguishable from each other and bulklike, including showing the gap. Strong interactions between the interface O and the Fe_B layers resulting from hybridization of the O $2p$ and Fe_B $3d$ orbitals strongly modify the interface O LDOS, including forming states around the Fermi level. Because of the large Fe magnetic moment ($\sim 3.5\mu_B$ inside the atomic sphere), there is a transferred magnetic moment of $\sim 0.15\mu_B$ on the interface O, leading not only to shifts of the LDOS for the different spin directions, but also to significant changes in the majority and minority O LDOS. (Because of the large Fe magnetic moment, there are fewer minority Fe states to hybridize with the oxygen states, leading to these magnetically induced changes.) For the next oxygen layer in the Fe_3O_4 (O:Fe_3O_4), although there is still a noticeable difference between the LDOS of the two oxygen sites, the electronic structure is already reasonably bulklike, including the magnetic properties. These comparisons of the LDOS around the O—Fe_B interface suggest that the polarity "problem" long associated with polar interfaces is basically solved within the first few layers around the O—Fe interface.

IV. CONCLUSIONS

We have presented a study of the atomic and electronic structure of the model epitaxial Fe_3O_4(111)/MgO(111) polar

oxide interface, combining experimental and theoretical HR-TEM studies with first-principles DFT calculations. The experimental images rule out interface faceting as a possible stabilization mechanism, and indicate that the $Fe_3O_4(111)$ film has a preferred stacking, implying a unique atomic interface structure. Furthermore, the DFT calculations rule out interface mixing as a stabilization mechanism. Comparisons of experimental atomic resolution images and calculated HR-TEM images for four model interfaces (B, ABA, BA, and A) finds that interface B is the best fit to experiment: the structure of the interface is an 1×1 O-termination of the polar MgO substrate, with the growth of the magnetite film initiated by a monolayer of Fe in the octahedral (B) position, i.e., …4Mg/4O/3Fe_B/4O/Fe_A/Fe_B/Fe_A/4O… This model is also the preferred model based on the DFT calculations. The models initiating with a full iron triple layer (4O/Fe_A/Fe_B/Fe_A/4O), or some fraction of this triple layer (e.g., 4O/Fe_B/Fe_A/4O and 4O/Fe_A/4O), neither fit experiment as well nor are calculated to be energetically favorable.

Calculations of the electronic structure predict strong bonding across the polar oxide interface, with metallic states present in the band gap of the O interface layers. These states are found to be rather localized at the interface and the LDOS already within a few layers of the interface are remarkably bulklike. Thus, the effects of the electrostatic mismatch due to the interface polarity (dipole moments) are removed within the first few interface layers, suggesting that the electronic screening of the interface dipoles is very effective. This electronic screening may allow atomically abrupt interfaces, in marked contrast to classical electrostatic models that require atomic mixing at polar interfaces. Finally, we have shown that the polarity of the substrate has an important effect on the growth of the $Fe_3O_4(111)$/MgO(111) polar interface by strongly favoring the B interface over the ABA one, a result closely related to the recently found[18] ability to selectively grow the cubic and hexagonal forms of GaN on MgO(111) by altering the interface structure by changing the initial conditions of the oxide surface. The present results, together with those for GaN—MgO, demonstrate that the initial stage of growth at a polar interface can play the defining role in determining the overall structure even for thick films and that this initial growth is strongly influenced by the polar nature of the interfaces.

ACKNOWLEDGMENTS

The study at the University of Wisconsin Milwaukee (UWM) was sponsored by the National Science Foundation Presidential Faculty (MGJ: NSF/DMR-95531489), the Research Corporation Advanced Opportunity (MGJ: RA0331), and the UWM Research Foundation grant (MW). The MBE growth of the studied model polar oxide system was performed at the Environmental Molecular Sciences Laboratory, a national scientific user facility sponsored by the Department of Energy's Office of Biological and Environmental Research located at Pacific Northwest National Laboratory.

*Present address: Brookhaven National Lab, 50 Bell Ave. BLD#463, Upton, NY 11973-5000.

†Corresponding author. Mailing address: Department of Physics, UWM, 1900 E. Kenwood Blvd., Room 323, Milwaukee, WI 53211. FAX: 414-229-5589; Email address: mgj@uwm.edu

[1] C. Noguera, J. Phys.: Condens. Matter **12**, R367 (2000).

[2] W. A. Harrison, E. A. Kraut, J. R. Waldrop, and R. W. Grant, Phys. Rev. B **18**, 4402 (1978).

[3] F. A. Ponce, C. G. Van de Walle, and J. E. Northrup, Phys. Rev. B **53** 7473 (1996).

[4] V. K. Lazarov, S. A. Chambers, and M. Gajdardziska-Josifovska, Phys. Rev. Lett. **90**, 216108 (2003).

[5] S. A. Chambers, Surf. Sci. Rep. **39**, 105 (2000).

[6] W. Weiss, A. Barbieri, M. A. Van Hove, and G. A. Samorjai, Phys. Rev. Lett. **71**, 1848 (1993).

[7] S. A. Chambers, S. Thevuthasan, and S. Joyce, Surf. Sci. **450**, L273 (2000).

[8] B. Stanka, W. Hebenstreit, U. Diebold, and S. A. Chambers, Surf. Sci. **448**, 49 (2000).

[9] R. F. C. Farrow, P. M. Rice, M. F. Toney, R. F. Marks, J. A. Hedstrom, R. Stephenson, M. J. Carey, and A. J. Kellock, J. Appl. Phys. **93**, 5626 (2003).

[10] V. K. Lazarov, R. Plass, H-C. Poon, D. K. Saldin, M. Weinert, S. A. Chambers, and M. Gajdardziska-Josifovska, Phys. Rev. B **71**, 115434 (2005).

[11] J. M. Cowley and A. F. Moodie, Acta Crystallogr. **10**, 390 (1957).

[12] P. Stadelmann, Ultramicroscopy **21**, 131 (1987).

[13] E. Wimmer, H. Krakauer, M. Weinert, and A. J. Freeman, Phys. Rev. B **24**, 864 (1981); M. Weinert, E. Wimmer, and A. J. Freeman, *ibid.* **26**, 4571 (1982); M. Weinert, G. Schneider, R. Podloucky, and J. Redinger, http://www.uwm.edu/~weinert/flair.html

[14] J. P. Perdew, K. Burke, and M. Ernzerhof, Phys. Rev. Lett. **77**, 3865 (1996); **78**, 1396(E) (1997).

[15] V. K. Lazarov, Ph.D. dissertation, University of Wisconsin Milwaukee, 2004.

[16] B. N. Sverdlov, G. A. Martin, H. Marcoc, and D. J. Smith, Appl. Phys. Lett. **67**, 2063 (1995).

[17] E. Wimmer, A. J. Freeman, M. Weinert, H. Krakauer, J. R. Hiskes, and A. M. Karo, Phys. Rev. Lett. **48**, 1128 (1982).

[18] V. K. Lazarov, J. Zimmermann, S. H. Cheung, L. Li, M. Weinert, and M. Gajdardziska-Josifovska, Phys. Rev. Lett. **94**, 216101 (2005).